

Unusual slow magnetic fluctuations and critical slowing down in
 $\text{Sr}_2\text{Ir}_{1-x}\text{Rh}_x\text{O}_4$

C. Tan,¹ Z. F. Ding,¹ J. Zhang,¹ Z. H. Zhu,¹ O. O. Bernal,² P. C. Ho,³ A. D. Hillier,⁴
A. Koda,⁵ H. Luetkens,⁶ G. D. Morris,⁷ D. E. MacLaughlin,⁸ and L. Shu^{1,9,*}

¹*State Key Laboratory of Surface Physics, Department of Physics,
Fudan University, Shanghai 200433, China*

²*Department of Physics and Astronomy,
California State University, Los Angeles, California 90032, USA*

³*Department of Physics, California State University, Fresno, California 93740, USA*

⁴*ISIS Facility, STFC Rutherford Appleton Laboratory,
Harwell Science and Innovation Campus,
Chilton, Didcot, Oxon, United Kingdom*

⁵*Institute of Materials Structure Science,
High Energy Accelerator Research Organization(KEK), Tokai, Ibaraki, 319-1106, Japan.*

⁶*Laboratory for Muon-Spin Spectroscopy,
Paul Scherrer Institut, 5232 Villigen, Switzerland*

⁷*Centre for Molecular and Materials Science, TRIUMF,
Vancouver, British Columbia V6T 2A3, Canada*

⁸*Department of Physics and Astronomy,
University of California, Riverside, California 92521, USA*

⁹*Collaborative Innovation Center of Advanced Microstructures, Nanjing 210093, China*

(Dated: October 18, 2019)

Abstract

Hidden magnetic order of $\text{Sr}_2\text{Ir}_{1-x}\text{Rh}_x\text{O}_4$, $x = 0.05$ and 0.1 , has been studied using muon spin relaxation spectroscopy. In zero applied field and weak longitudinal fields ($\mu_0 H_L \lesssim 2$ mT), muon spin relaxation data can be well described by exponentially-damped static Lorentzian Kubo-Toyabe functions, indicating that static and dynamic local fields coexist at each muon site. For $\mu_0 H_L \gtrsim 2$ mT, the static rate is completely decoupled, and the exponential decay is due to dynamic spin fluctuations. In both zero field and $\mu_0 H_L = 1-2$ mT, the temperature dependencies of the exponential muon spin relaxation rate exhibit maxima at 215 K for $x = 0.05$ and 175 K for $x = 0.1$, suggesting critical slowing down of electronic spin fluctuations. The field dependencies of the dynamic spin fluctuation rates can be well described by the Redfield relation. The correlation time of this electronic spin fluctuation is in the range of 2–5 ns for $\text{Sr}_2\text{Ir}_{0.9}\text{Rh}_{0.1}\text{O}_4$, and shorter than 2 ns for $\text{Sr}_2\text{Ir}_{0.95}\text{Rh}_{0.05}\text{O}_4$. The rms fluctuating field is on the order of 1 mT, which is consistent with the polarized neutron diffraction cross-section.

* Corresponding author: leishu@fudan.edu.cn

I. INTRODUCTION

Iridium oxides have attracted growing attention because their physical properties can be significantly influenced by the combination of strong spin-orbit interactions and electron correlations. Sr_2IrO_4 , an archetypal $J_{\text{eff}} = 1/2$ Mott insulator, has structural, electronic, and magnetic properties similar to those of the $S = 1/2$ Mott insulator La_2CuO_4 [1–5]. Fermi arcs and a V-shaped low-energy gap in electron-doped Sr_2IrO_4 remarkably resemble the properties of hole-doped cuprate superconductors [6–9]. Theoretical predictions and empirical experimental observations suggest that doped Sr_2IrO_4 is a promising system for comparison with cuprates, and may even possess new states of matter [1, 10].

Recently an odd-parity hidden order, which breaks spatial inversion and rotational symmetry, was inferred from an optical second harmonic generation (SHG) study of undoped and Rh-doped Sr_2IrO_4 [11]. Polarized neutron diffraction (PND) further revealed that this order breaks time-reversal symmetry while preserving translation symmetry of the lattice [12]. The broken symmetries of this hidden magnetic order are consistent with the loop-current model [13] proposed to explain exotic properties of the pseudogap state in cuprates [14].

The nature of the pseudogap state is a fascinating puzzle in condensed matter physics. The observation of spontaneous breaking of time-reversal symmetry in $\text{Bi}_2\text{Sr}_2\text{CaCu}_2\text{O}_{8+\delta}$ [15] provides evidence that the pseudogap is a novel phase rather than a crossover. The pioneering PND studies of Fauqué *et al.* on $\text{YBa}_2\text{Cu}_3\text{O}_{6+x}$ (YBCO) [16] revealed an intra-unit-cell (IUC) magnetic order (i.e., order that preserves lattice translational symmetry) in the pseudogap phase. A similar IUC magnetic order in the pseudogap phase was subsequently found in $\text{HgBa}_2\text{CuO}_{4+\delta}$ [17] and $\text{Bi}_2\text{Sr}_2\text{CaCu}_2\text{O}_{8+\delta}$ [18]. However, the absence of static magnetic fields with expected amplitude in nuclear magnetic resonance [19, 20] and muon spin relaxation/rotation (μSR) [21–24] experiments has raised doubts about the existence of IUC magnetic order. Recently, Zhang *et al.* [25] discovered slow magnetic fluctuations in YBCO via the field dependence of the dynamic muon spin relaxation rate, demonstrating magnetic order in the pseudogap phase of this system. The correlation time τ_c of these fluctuations is on the order of 10^{-9} s, so that they are static on the neutron time scale (10^{-11} s) [12].

The μSR technique [26–28] is unmatched in its sensitivity to magnetic field on the local (atomic) scale. In particular, μSR is capable of detecting nearby static magnetic moments in the range of 0.001–0.01 μ_B , and it can measure correlation time of magnetic fluctuations in the range

of 10^{-4} to 10^{-12} s, depending on the magnitude of magnetic fields at muon sites. Since the hidden-order phase in $\text{Sr}_2\text{Ir}_{1-x}\text{Rh}_x\text{O}_4$ resembles that in the pseudogap state of cuprates, the hidden-order magnetism might also fluctuate with a comparable time scale in $\text{Sr}_2\text{Ir}_{1-x}\text{Rh}_x\text{O}_4$. μSR should be a suitable probe to detect such fluctuations.

Using zero field (ZF) and longitudinal field (LF) μSR techniques, here we report the observation of slow spin dynamics with a time scale of 10^{-9} s, comparable to the fluctuation rate in cuprates [25]. These results suggest a similar origin of electronic spin dynamics. The temperature dependencies of ZF and LF relaxation rates exhibit maxima at a temperature T^* , consistent with the hidden order temperature observed in SHG [11] and PND [12] experiments. We interpret this result as further evidence for the hidden order revealed by the SHG and PND studies [11, 12].

II. METHODS

Single crystals of $\text{Sr}_2\text{Ir}_{1-x}\text{Rh}_x\text{O}_4$, $x = 0.05$ and 0.1 , were grown from off-stoichiometric quantities of SrCl_2 , SrCO_3 , IrO_2 , and RhO_2 using a self-flux method. Details of the method are described elsewhere [29]. The average size of the crystals is $1 \times 1 \times 0.2$ mm³, with the 1×1 surface in the ab plane [30]. Powder X-ray diffraction, magnetic susceptibility, and resistivity measurements were performed on a Bruker DISCOVER 8 diffractometer, a Quantum Design SQUID magnetometer, and a Quantum Design physical properties measurement system, respectively. ZF-, LF-, and weak transverse field (wTF) μSR experiments were performed using the ISIS EMU spectrometer at Rutherford Appleton Laboratory, Didcot, U.K., the S1 spectrometer at J-PARC, Tokai, Japan, and the GPS spectrometer at the Paul Scherrer Institute, Villigen, Switzerland.

A. The SR technique

In the time-differential μSR technique [26–28], the time evolution of the ensemble muon spin polarization $G(t)$ in a sample is obtained from measurements of the *asymmetry spectrum* $A(t)$ in count rates of beta-decay positrons, where t is the time after muon implantation. In general $A(t) = A_0 G(t)$, where the initial asymmetry A_0 depends on spectrometer details but is roughly 0.2. The behavior of local fields at muon sites due to nuclear and electronic magnetism is reflected in the form of $G(t)$. Relaxation (loss of muon polarization) is due to dephasing of muon precession in a distribution of static local fields, dynamic fluctuations of local fields, or a combination of these;

often the form of the static local field distribution can be determined.

Nuclear magnetism usually results in dipolar fields that are quasistatic (slow compared to the relevant time scale), since nuclear spin fluctuations normally obey this condition [31]. For randomly-oriented quasistatic Gaussian and Lorentzian field distributions, the ZF muon spin polarization functions $G(t)$ are given by [31]

$$G_{ZF}^{\text{Gauss}}(t) = \frac{1}{3} + \frac{2}{3} [1 - (\sigma t)^2] \exp[-\frac{1}{2}(\sigma t)^2] \quad (\text{Gaussian}) \quad (1)$$

and [32]

$$G_{ZF}^{\text{Lor}}(t) = \frac{1}{3} + \frac{2}{3}(1 - \lambda t) \exp(-\lambda t) \quad (\text{Lorentzian}), \quad (2)$$

respectively. These are examples of so-called Kubo-Toyabe (KT) relaxation functions [33]. Static muon spin relaxation can be “decoupled” by applying a sufficiently strong longitudinal field, since then the resultant field is nearly parallel to the initial muon polarization and there is little precession. We denote a static LF KT polarization function by $G_{LF}^{\text{Gauss}}(t)$ [31] or $G_{LF}^{\text{Lor}}(t)$ [32].

Dynamic muon spin relaxation is caused by fluctuating local fields $B_{\text{loc}}(t)$ at muon sites. $G(t)$ depends on properties of B_{loc} , one of which is the correlation time τ_c that characterizes its stochastic time dependence. When $\gamma_\mu B_{\text{loc}}^{\text{rms}} \tau_c \ll 1$, where $\gamma_\mu/2\pi = 135.53$ MHz/T is the gyromagnetic ratio of the muon and $B_{\text{loc}}^{\text{rms}} = \langle B_{\text{loc}}^2(t) \rangle^{1/2}$ is the rms value of the local field, the relaxation is in the so-called “motional narrowing” limit. This results in $G(t)$ decays exponentially [$G(0) = 1$]:

$$G(t) = \exp(-\lambda t), \quad (3)$$

where the relaxation rate λ is of the order of $(\gamma_\mu B_{\text{loc}}^{\text{rms}})^2 \tau_c$, i.e., proportional to τ_c . In this limit, $\lambda \equiv \lambda_{ZF} = 2(\gamma_\mu B_{\text{loc}}^{\text{rms}})^2 \tau_c$ in ZF [28]. In a LF experiment, the field dependence of the relaxation rate $\lambda \equiv \lambda_{LF}$ is given by the Redfield relation [28, 34]

$$\lambda_{LF}(H_L) = \frac{2(\gamma_\mu B_{\text{loc}}^{\text{rms}})^2 \tau_c}{(\gamma_\mu H_L \tau_c)^2 + 1}. \quad (4)$$

This field dependence has been observed in a number of systems, including the high temperature superconductor YBCO [25] and the heavy fermion superconductor PrOs₄Sb₁₂ [35].

III. RESULTS

A. AFM state

wTF- μ SR can be used to determine the transition from the paramagnetic to the ordered magnetic state [28]. In a paramagnet, muon spins precess in the applied field at the Larmor frequency,

usually without strong depolarization. In the magnetically-ordered state, a broad distribution of static internal fields results in a rapid relaxation of the wTF muon polarization. Then any precessing signal at late times originates from the muons that miss the sample and stop in the sample holder [36]. The observed initial precessing asymmetry A_0 is the sum of both sample and silver asymmetries above T_N , but is only the silver asymmetry well below the transition.

Figure 1 shows the temperature dependence of the initial asymmetry A_0 of the precessing signal in $\text{Sr}_2\text{Ir}_{1-x}\text{Rh}_x\text{O}_4$, $x = 0.05$ and 0.1 , from fits to the late-time wTF spectra. Asymmetry loss

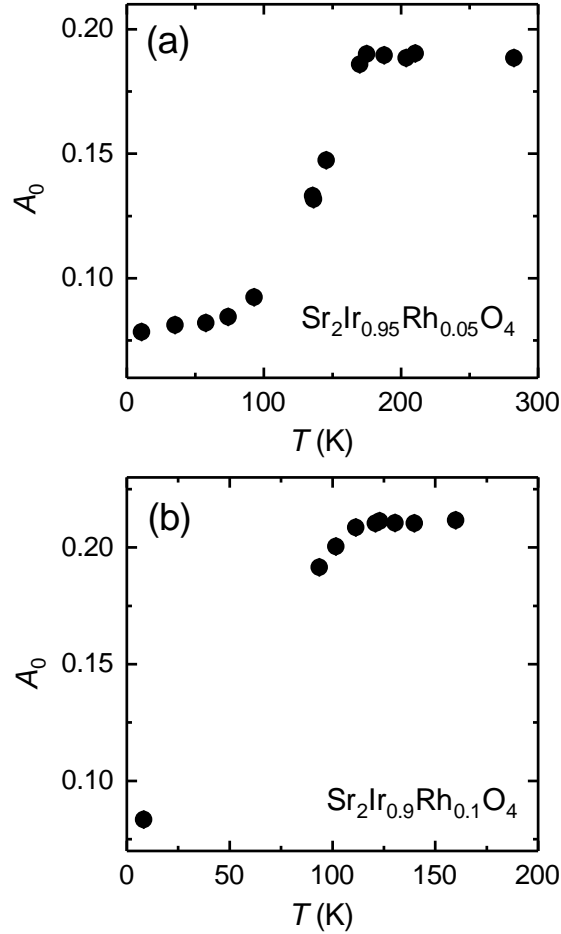


FIG. 1. Temperature dependence of the late-time initial asymmetry A_0 from wTF- μ SR asymmetry spectra in (a) $\text{Sr}_2\text{Ir}_{0.95}\text{Rh}_{0.05}\text{O}_4$ and (b) $\text{Sr}_2\text{Ir}_{0.9}\text{Rh}_{0.1}\text{O}_4$ (Data taken at J-PARC).

corresponding to the onset of AFM order is observed below Néel temperatures $T_N = 175(5)$ K and $110(5)$ K for $x = 0.05$ and 0.1 , respectively. These results agree well with previous determinations of T_N , as discussed in Sec. III B 2.

B. Paramagnetic state

1. Muon spin relaxation in ZF and low-field LF

Above T_N , the ZF muon spin depolarization can be well described by either Eq. (2) or Eq. (3). As discussed in Sec. II A, these two functions represent relaxation by static and dynamic muon local fields, respectively. To decide between these situations, low-field LF- μ SR experiments were performed. As shown in Fig. 2, the spectra exhibit strongly damped oscillations at the LF frequency, and the initial slopes of the spectra are field-independent. These are characteristic of a

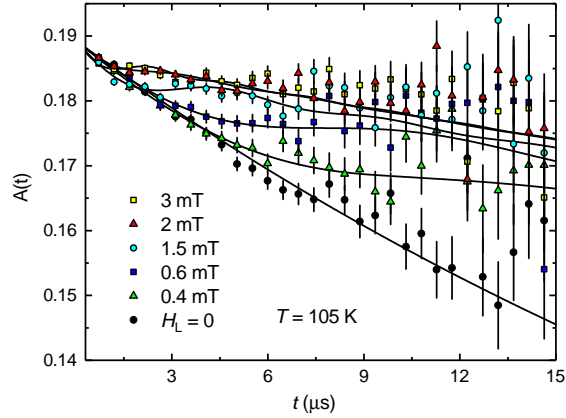


FIG. 2. ZF- and low-field LF- μ SR time spectra from $\text{Sr}_2\text{Ir}_{0.9}\text{Rh}_{0.1}\text{O}_4$ for various fields at 105 K (Data taken at J-PARC). Curves: fits of Eq. (5) to the LF data. The weakly-relaxing signal from muons that stop in the silver backing plate has not been subtracted.

static LF KT function [31]. There is hardly any difference between spectra at $\mu_0 H_L = 2$ mT and 3 mT, as expected from decoupling of static local fields. However, at these fields there is still relaxation with a significant value of the damping rate, which must be dynamic in nature.

Fits of the static LF Lorentzian KT function [32] with exponential damping

$$G(t) = G_{\text{LF}}^{\text{Lor}}(t)\exp(-\lambda_{\text{LF}}t), \quad (5)$$

shown in Fig. 2, and describe the data well at all fields. This function models the combined effects of static (nuclear) and dynamic (electronic) local fields that coexist as vector sums at the muon site(s) [32].

2. Temperature dependencies of the relaxation rates

In a weak LF, the asymmetry spectra are best described by Eq. (5). The two relaxation rates in this function are highly correlated statistically in the data, and cannot be separated. In particular, a simple exponential [Eq. (3)] provides good fits to ZF data, where λ_{ZF} is much larger than in high field and is therefore dominated by the static relaxation rate. In 10 or 20 mT LF, the static component is essentially decoupled [$G_{\text{LF}}^{\text{Lor}}(t) \simeq 1$], and the relaxation is again simple exponential. We also use Eq. (3) to fit LF data at higher fields, where $\lambda \equiv \lambda_{\text{LF}}$ is a dynamic relaxation rate.

Figure 3 gives the temperature dependencies of the exponential relaxation rates in $\text{Sr}_2\text{Ir}_{1-x}\text{Rh}_x\text{O}_4$, $x = 0.05$ and 0.1 , in ZF [Figs. 3(a) and (c)] and LF [Figs. 3(b) and (d)]; in the latter $\mu_0 H_L = 20$ mT and 10 mT were used for $x = 0.1$ and 0.05 , respectively. The temperature dependencies of the relaxation rates exhibit maxima at temperatures $T^*(x)$ in both ZF and LF. The presence of relaxation rate maxima suggests critical slowing down of dynamic magnetic fluctuations, with transitions at T^* . Below T^* , λ_{ZF} increases with decreasing temperature, whereas λ_{LF} is almost temperature independent. This suggests that the temperature dependence of λ_{ZF} at low temperature is due to the static rate.

Values of T_N from Fig. 1 and T^* from Figs. 3(a)–(d) are plotted on the magnetic phase diagram of $\text{Sr}_2\text{Ir}_{1-x}\text{Rh}_x\text{O}_4$ in Fig. 3(e). The values of T_N match well with dc magnetic susceptibility data [30], and T^* values agree with symmetry-breaking hidden-order transition temperatures obtained from SHG [11] and PND [12] experiments. The latter agreement provides strong evidence that the muon spin relaxation is due to fluctuations of the hidden order.

3. Field dependence of λ_{LF}

LF- μSR experiments above $\mu_0 H_L = 2$ mT were carried out in $\text{Sr}_2\text{Ir}_{1-x}\text{Rh}_x\text{O}_4$, $x = 0.05$ and 0.1 , at a number of different temperatures. As shown in Figs. 4(a)–(f), the field dependencies of λ_{LF} are well described by Eq. (4). The resulting fit parameters are shown in Table I.

For $x = 0.1$, $B_{\text{loc}}^{\text{rms}}$ and τ_c are relatively well determined. The relaxation is in the extreme motional narrowing limit: $\gamma_\mu B_{\text{loc}}^{\text{rms}} \tau_c \approx 3.6 \times 10^{-3}$. For $x = 0.05$ the field dependencies of λ_{LF} are not as clear as for $x = 0.1$, due to the very small values of the rates and the likelihood that τ_c is too short to allow the decrease in λ_{LF} for $\gamma_\mu H_L \tau_c > 1$ [Eq. (4)] to be well resolved with the highest available field. The 188-K data are hard to fit with both $B_{\text{loc}}^{\text{rms}}$ and τ_c free without data from higher

TABLE I. rms muon local fields $B_{\text{loc}}^{\text{rms}}$ and correlation times τ_c for $\text{Sr}_2\text{Ir}_{0.9}\text{Rh}_{0.1}\text{O}_4$ and $\text{Sr}_2\text{Ir}_{0.95}\text{Rh}_{0.05}\text{O}_4$ from fits of Eq. (4) to the data of Fig. 4.

Rh concentration	T (K)	$B_{\text{loc}}^{\text{rms}}$ (mT)	τ_c (ns)
0.1	90 K	0.84(8)	4.0(9)
0.1	105 K	1.0(7)	4(1)
0.1	120 K	0.9(1)	2.8(8)
0.1	142 K	0.85(4)	3.8(4)
0.1	160 K	1.3(3)	1.5(7)
0.1	175 K	1.3(1)	3.0(4)
0.05	173 K	0.8(1)	3(1)
0.05	188 K	1.2(fix)	1.3(1)

fields ($\mu_0 H_L > 400$ mT); $B_{\text{loc}}^{\text{rms}}$ was fixed at 1.2 mT to obtain an estimated correlation time that is shorter than 2 ns.

The observed small relaxation rates are close to the limit of the μSR technique [38], and their uncertainties are large, as are those of the fitted parameters from Eq. (4); the data of Table I do not exhibit a systematic temperature dependence. Rough values of $B_{\text{loc}}^{\text{rms}}$ and τ_c are obtained for both Rh concentrations.

IV. DISCUSSION

A. Comparison with other experiments and theory

As noted above, the observed values of the peak temperatures T^* are in good agreement with the results of SHG [11] and PND [12] experiments. Fauqué *et al.* [16] reported that in YBCO the neutron scattering cross section of the IUC order is $\sim 1\text{--}2$ mbarns/formula unit, from which they deduced an ordered magnetic moment of $0.05\text{--}0.1 \mu_B$. Based on dipolar lattice-sum calculations, Zhang *et al.* [21, 25] estimated B_{loc} to be 1 to 1.5 mT for $0.1\text{--}\mu_B$ IUC moments. For $\text{Sr}_2\text{Ir}_{1-x}\text{Rh}_x\text{O}_4$, the magnetic cross-section of hidden magnetic order was estimated as ~ 2 mbarns per formula unit [12]. The 1-mT values of $B_{\text{loc}}^{\text{rms}}$ for $\text{Sr}_2\text{Ir}_{1-x}\text{Rh}_x\text{O}_4$ are therefore roughly consistent with the PND results [11].

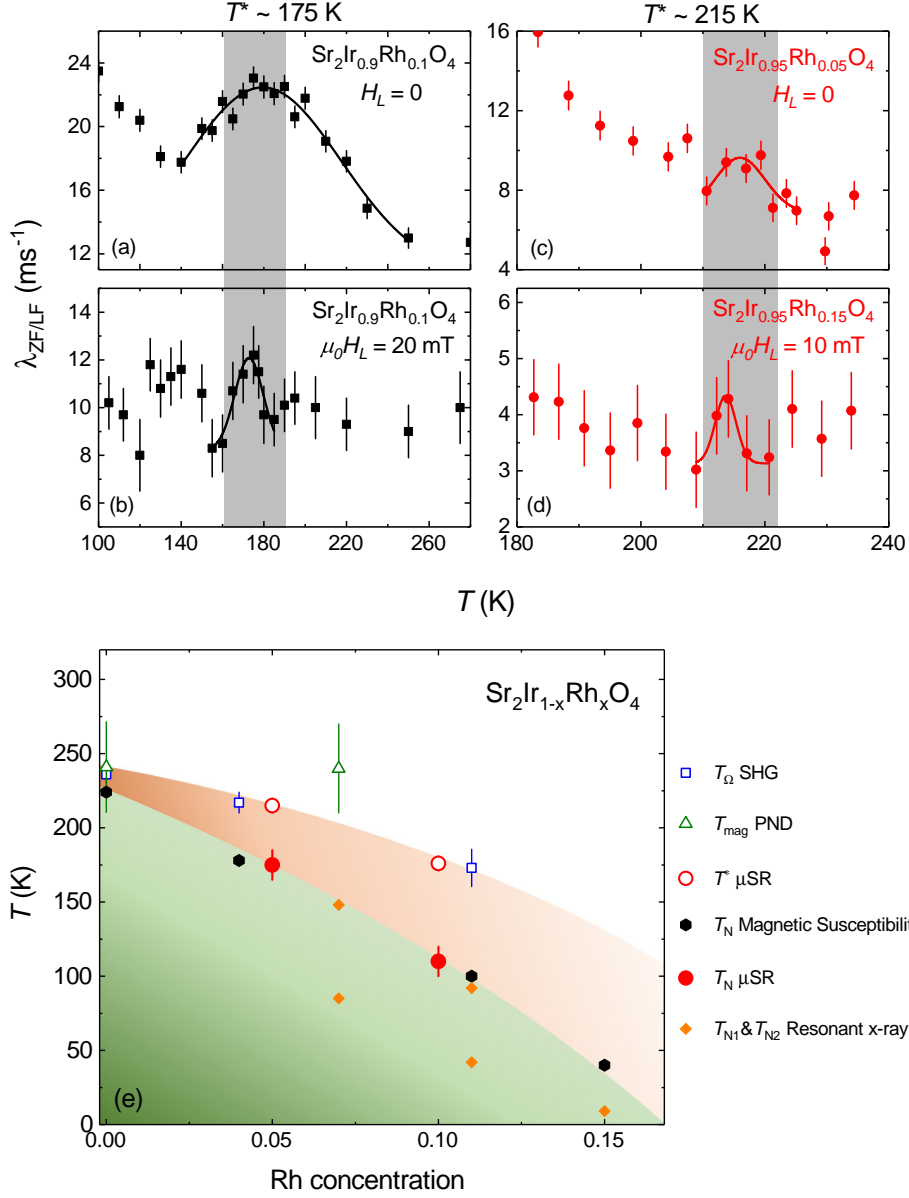


FIG. 3. Temperature dependencies of ZF and LF muon spin relaxation rates in $\text{Sr}_2\text{Ir}_{1-x}\text{Rh}_x\text{O}_4$. (a) $x = 0.1$, $H_L = 0$ (Data taken at ISIS). (b) $x = 0.1$, $\mu_0 H_L = 20$ mT (Data taken at PSI). (c) $x = 0.05$, $H_L = 0$ (Data taken at J-PARC). (d) $x = 0.05$, $\mu_0 H_L = 10$ mT (Data taken at J-PARC). The curves are guides to the eye. Gray areas: uncertainty in T^* from previous reports [11, 12]. (e) Magnetic phase diagram of $\text{Sr}_2\text{Ir}_{1-x}\text{Rh}_x\text{O}_4$. Filled circles: Néel temperature T_N from μ SR (this work). Hexagons: T_N from magnetic susceptibility [30]. Diamonds: long-range and short-range T_N from resonant x-ray diffraction [37]. Open circles: hidden order transition temperature T^* from μ SR (this work). Squares: T_{Ω} from second harmonic generation [11]. Triangles: T_{mag} from polarized neutron diffraction [12].

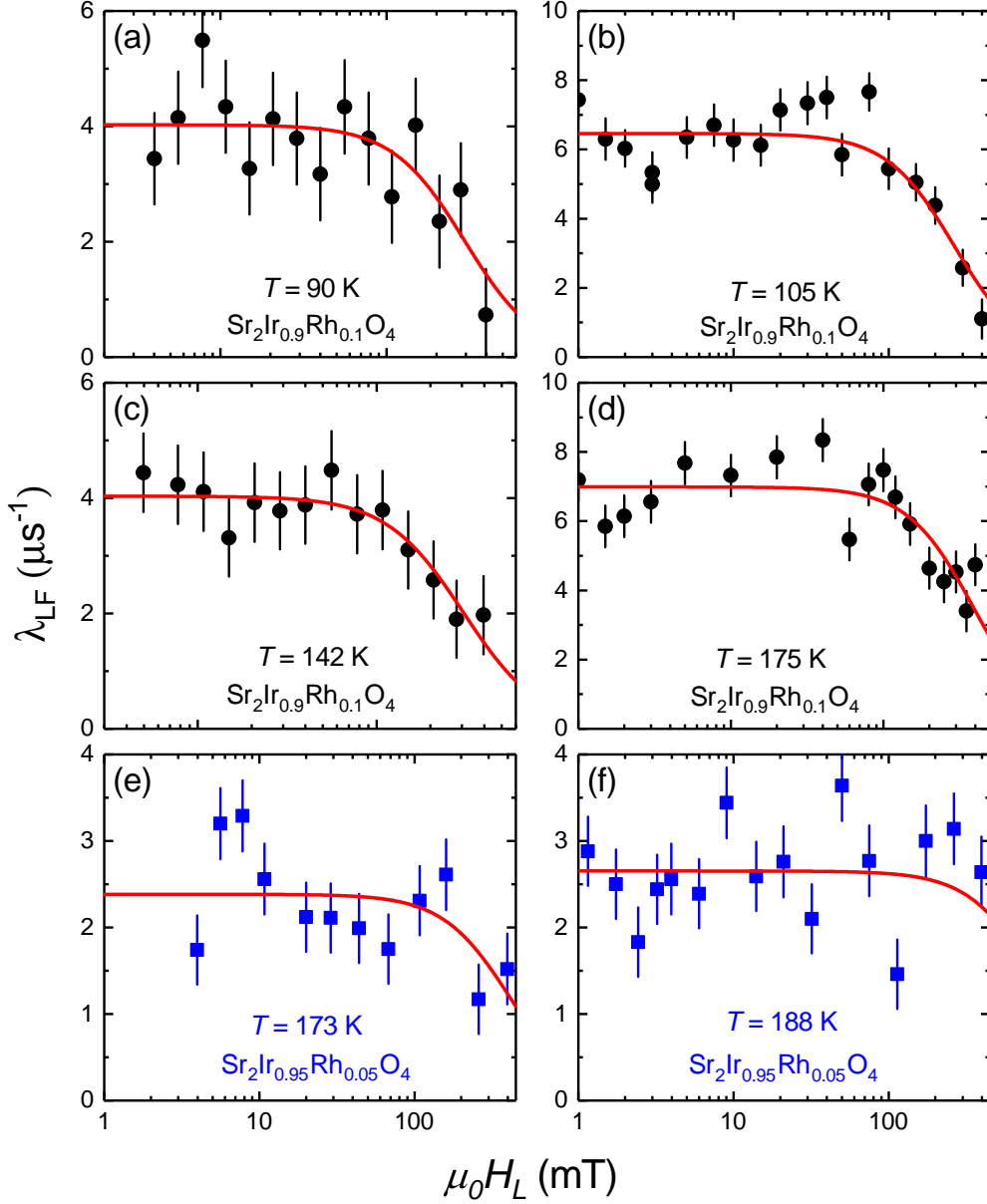


FIG. 4. Field dependence of LF relaxation rate $\lambda_{\text{LF}}(H_L)$ in $\text{Sr}_2\text{Ir}_{1-x}\text{Rh}_x\text{O}_4$, $\mu_0 H_L \geq 2$ mT. (a) $x = 0.1$, $T = 90$ K (Data taken at J-PARC). (b) $x = 0.1$, $T = 105$ K (Data taken at ISIS). (c) $x = 0.1$, $T = 142$ K (Data taken at J-PARC). (d) $x = 0.1$, $T = 175$ K (Data taken at ISIS). (e) $x = 0.05$, $T = 173$ K (Data taken at J-PARC). (f) $T = 188$ K (Data taken at J-PARC). Curves: fits of Eq. (4) to the data [$B_{\text{loc}}^{\text{rms}}$ was fixed at 1.2 mT for (f) $x = 0.05$, $T = 188$ K].

Compared to SHG and PND experiments [11, 12], μ SR characterizes T^* from a different aspect: critical slowing down, evidenced by relaxation rate maxima at T^* . However, static magnetism does not set in below T^* as it would for a conventional phase transition. Muon spin relaxation but no static magnetism below T^* has also been observed in YBCO [25], and has been associated with fluctuations of IUC magnetic order. In the loop-current theory of Varma [39], loop-current order forms domains with a finite correlation length and consequent low-frequency excitations at all temperatures; these are quasistatic on the PND time scale but prevent truly static order. This behavior is suggested by our μ SR results, but quantitative comparison must await further development of such a theory.

B. Origin of the peaks in λ_{LF}

The relaxation-rate maxima in Figs. 3(a)–(d) suggest critical slowing down and a phase transition at T^* , but they might alternatively be due to a passage through a so-called “BPP peak” [40], i.e., the maximum in Eq. (4) as a function of τ_c at $\tau_c = 1/\gamma_\mu H_L$. In this scenario τ_c varies monotonically with temperature, and T^* is not a transition temperature.

We test such a hypothesis by comparing Eq. (4) with the observed τ_c . Figure 5 shows the calculated dependence of the relaxation rate λ_{LF} on τ_c from Eq. (4) for $\mu_0 H_L = 20$ mT, $B_{loc}^{rms} = 1$ mT; and $\mu_0 H_L = 10$ mT, $B_{loc}^{rms} = 1.2$ mT [Figs. 3(a)–(d)]. The yellow and cyan areas represent

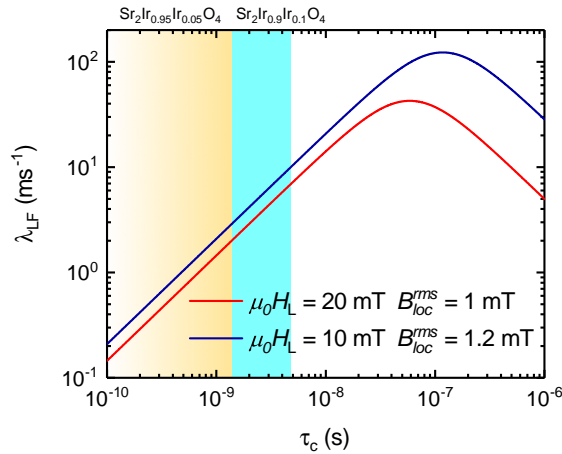


FIG. 5. Calculated relaxation rate from Eq. (4) for $\mu_0 H_L = 20$ mT, $B_{loc}^{rms} = 1$ mT ($x = 0.1$, red) and $\mu_0 H_L = 10$ mT, $B_{loc}^{rms} = 1.2$ mT ($x = 0.05$, blue). The ranges of estimated τ_c values are given by the light cyan area for $x = 0.1$ and the yellow area for $x = 0.05$.

the ranges of estimated τ_c values for $x = 0.05$ and 0.1 , respectively. In these ranges λ_{LF} varies monotonically with τ_c . This rules out the possibility that the maxima of $\lambda_{\text{LF}}(T)$ at T^* are due to a passage through the BPP peak, and confirms that the maxima are due to critical slowing down.

The relaxation rate of $\text{Sr}_2\text{Ir}_{0.95}\text{Rh}_{0.05}\text{O}_4$ is smaller than that of $\text{Sr}_2\text{Ir}_{0.9}\text{Rh}_{0.1}\text{O}_4$, which explains in part why the maxima in Figs. 3(c) and (d) are not as significant as those in Figs. 3(a) and (b). The correlation time τ_c increases with increasing x , similar to the dependence of τ_c on the oxygen content y in $\text{YBa}_2\text{Cu}_3\text{O}_y$ [25] and suggesting τ_c depends on the hole or electron concentration rather than defects.

C. Static muon relaxation rate

In Sec. III B 1, we concluded that the low-field behavior of the muon relaxation is well described by Eq. (5) assuming a Lorentzian nuclear dipolar field distribution. This is in contrast with the Gaussian distribution that is normally expected from nuclear fields [31]. In $\text{Sr}_2\text{Ir}_{1-x}\text{Rh}_x\text{O}_4$ the nuclear dipolar fields are mainly due to Rh and Ir nuclear isotopes with considerably different nuclear magnetic moments (Ref. 28, Appendix G). This additional disorder is presumably responsible for the Lorentzian-like field distribution. A Lorentzian nuclear field distribution was also observed in the cuprate-analog nickelate $\text{La}_4\text{Ni}_3\text{O}_8$ [41] and attributed to the large number of candidate muon stopping sites. The value of λ_{ZF} for $\text{Sr}_2\text{Ir}_{0.9}\text{Rh}_{0.1}\text{O}_4$ is about $0.02 \mu\text{s}^{-1}$ at 105 K. This is consistent with a rough estimate based on $^{191,193}\text{Ir}$ and ^{103}Rh nuclear moments and isotopic abundances. A quantitative comparison would require knowledge of muon stopping sites, which is currently unavailable.

The quasistatic muon relaxation rate due to nuclear dipolar fields is usually temperature-independent at low temperatures, with a decrease with increasing temperature due to the onset of thermally-activated muon diffusion [26–28]. As shown in Figs. 3(a) and (c), λ_{ZF} exhibits such a decrease underneath the relaxation rate maxima. The observed temperature dependence qualitatively resembles that in copper [42].

D. Statistical analysis

The statistical significance of the peaks in $\lambda(T)$ [Figs. 3(a)–(d)] is not large, and it requires further discussion. Following the treatment of Ref. 25, we define the inverse relative standard

deviation (IRSD) (the N in “ $N\sigma$ ”) for each peak as follows: a baseline is drawn between points chosen above and below the peak. The IRSD for the peak is then $[\sum_i A_i |A_i| / \sigma_i^2]^{1/2}$, where the sum is over the points in the peak, A_i is the point amplitude relative to the baseline, and σ_i is the point standard deviation. The sign of A_i is included to account for negative contributions.

The results are shown in Table II. It can be seen that the ZF IRSD for $x = 0.1$ is very large;

TABLE II. IRSDs of relaxation rate maxima near T^* from muon spin relaxation rate in $\text{Sr}_2\text{Ir}_{1-x}\text{Rh}_x\text{O}_4$.

x	$\mu_0 H_T$ (mT)	No. of points	IRSD	
0.1	0	17	28.2	Fig. 3(a)
	20	8	4.4	Fig. 3(b)
0.05	0	7	4.8	Fig. 3(c)
	10	5	2.2	Fig. 3(d)

this and the width of that peak are not understood. The other values are reasonable, given the crudeness of the procedure.

V. CONCLUSIONS

Our μSR study of the $\text{Sr}_2\text{Ir}_{1-x}\text{Rh}_x\text{O}_4$ system has revealed slow electronic magnetic fluctuations associated with the hidden magnetic order discovered in SHG [11] and PND [12] experiments. The temperature dependencies of the zero-field and longitudinal-field dynamic relaxation rates $\lambda_{\text{ZF}}(T)$ and $\lambda_{\text{LF}}(T)$ exhibit maxima near the hidden-order transition temperatures T^* found in SHG [11] and PND [12] experiments, suggesting critical slowing down of magnetic fluctuations, followed by a transition to a state characterized by fluctuations of the hidden order parameter. The field dependencies of λ_{LF} are well described by the Redfield relation [Eq. (4)], fits to which yield estimated correlation times in the range of 2–5 ns for $\text{Sr}_2\text{Ir}_{0.9}\text{Rh}_{0.1}\text{O}_4$ and shorter than 2 ns for $\text{Sr}_2\text{Ir}_{0.95}\text{Rh}_{0.05}\text{O}_4$. These results are quite similar to those observed in the YBCO system [25].

ACKNOWLEDGMENTS

We are grateful to C.M. Varma and R. Kadono for helpful discussions. This research was supported by the National Key Research and Development Program of China, No. 2017YFA0303104

and No. 2016YFA0300503, the National Natural Science Foundation of China, No. 11774061, the U.S. National Science Foundation, No. DMR/PREM-1523588, No. HRD-1547723 and No. DMR-1506677, and by the University of California, Riverside, Academic Senate.

- [1] F. Wang and T. Senthil, *Phys. Rev. Lett.* **106**, 136402 (2011).
- [2] H. Watanabe, T. Shirakawa, and S. Yunoki, *Phys. Rev. Lett.* **110**, 027002 (2013).
- [3] Z. Y. Meng, Y. B. Kim, and H.-Y. Kee, *Phys. Rev. Lett.* **113**, 177003 (2014).
- [4] F. Ye, S. Chi, B. C. Chakoumakos, J. A. Fernandez-Baca, T. Qi, and G. Cao, *Phys. Rev. B* **87**, 140406 (2013).
- [5] C. Dhital, T. Hogan, Z. Yamani, C. de la Cruz, X. Chen, S. Khadka, Z. Ren, and S. D. Wilson, *Phys. Rev. B* **87**, 144405 (2013).
- [6] Y. K. Kim, O. Krupin, J. D. Denlinger, A. Bostwick, E. Rotenberg, Q. Zhao, J. F. Mitchell, J. W. Allen, and B. J. Kim, *Science* **345**, 187 (2014).
- [7] A. de la Torre, S. McKeown Walker, F. Y. Bruno, S. Ricco, Z. Wang, I. Gutierrez Lezama, G. Scheerer, G. Giriat, D. Jaccard, C. Berthod, T. K. Kim, M. Hoesch, E. C. Hunter, R. S. Perry, A. Tamai, and F. Baumberger, *Phys. Rev. Lett.* **115**, 176402 (2015).
- [8] Y. J. Yan, M. Q. Ren, H. C. Xu, B. P. Xie, R. Tao, H. Y. Choi, N. Lee, Y. J. Choi, T. Zhang, and D. L. Feng, *Phys. Rev. X* **5**, 041018 (2015).
- [9] Y. K. Kim, N. H. Sung, J. D. Denlinger, and B. J. Kim, *Nature Phys.* **12**, 37 (2015).
- [10] S. Chikara, G. Fabbris, J. Terzic, G. Cao, D. Khomskii, and D. Haskel, *Phys. Rev. B* **95**, 060407 (2017).
- [11] L. Zhao, D. H. Torchinsky, H. Chu, V. Ivanov, R. Lifshitz, R. Flint, T. Qi, G. Cao, and D. Hsieh, *Nature Phys.* **12**, 32 (2015).
- [12] J. Jeong, Y. Sidis, A. Louat, V. Brouet, and P. Bourges, *Nat. Commun.* **8**, 15119 (2017).
- [13] C. M. Varma, *Phys. Rev. B* **55**, 14554 (1997); *Phys. Rev. B* **73**, 155113 (2006).
- [14] T. Timusk and B. Statt, *Rep. Progr. Phys.* **62**, 61 (1999).
- [15] A. Kaminski, S. Rosenkranz, H. M. Fretwell, J. C. Campuzano, Z. Li, H. Raffy, W. G. Cullen, H. You, C. G. Olson, C. M. Varma, and H. Hochst, *Nature* **416**, 610 (2002).
- [16] B. Fauque, Y. Sidis, V. Hinkov, S. Pailhes, C. T. Lin, X. Chaud, and P. Bourges, *Phys. Rev. Lett.* **96**, 197001 (2006).

- [17] Y. Li, V. Baledent, N. Barišić, Y. Cho, B. Fauqué, Y. Sidis, G. Yu, X. Zhao, P. Bourges, and M. Greven, *Nature* **455**, 372 (2008).
- [18] S. De Almeida-Didry, Y. Sidis, V. Balédent, F. Giovannelli, I. Monot-Laffez, and P. Bourges, *Phys. Rev. B* **86**, 020504 (2012).
- [19] A. M. Mounce, S. Oh, J. A. Lee, W. P. Halperin, A. P. Reyes, P. L. Kuhns, M. K. Chan, C. Dorow, L. Ji, D. Xia, X. Zhao, and M. Greven, *Phys. Rev. Lett.* **111**, 187003 (2013).
- [20] T. Wu, H. Mayaffre, S. Kramer, M. Horvatic, C. Berthier, W. N. Hardy, R. Liang, D. A. Bonn, and M. H. Julien, *Nat. Commun.* **6**, 6438 (2015).
- [21] G. J. MacDougall, A. A. Aczel, J. P. Carlo, T. Ito, J. Rodriguez, P. L. Russo, Y. J. Uemura, S. Wakimoto, and G. M. Luke, *Phys. Rev. Lett.* **101**, 017001 (2008).
- [22] J. E. Sonier, V. Pacradouni, S. A. Sabok-Sayr, W. N. Hardy, D. A. Bonn, R. Liang, and H. A. Mook, *Phys. Rev. Lett.* **103**, 167002 (2009).
- [23] W. Huang, V. Pacradouni, M. P. Kennett, S. Komiya, and J. E. Sonier, *Phys. Rev. B* **85**, 104527 (2012).
- [24] A. Pal, K. Akintola, M. Potma, M. Ishikado, H. Eisaki, W. N. Hardy, D. A. Bonn, R. Liang, and J. E. Sonier, *Phys. Rev. B* **94**, 134514 (2016).
- [25] J. Zhang, Z. Ding, C. Tan, K. Huang, O. O. Bernal, P.-C. Ho, G. D. Morris, A. D. Hillier, P. K. Biswas, S. P. Cottrell, H. Xiang, X. Yao, D. E. MacLaughlin, and L. Shu, *Sci. Adv.* **4**, eaao5235 (2018).
- [26] A. Schenck, *Muon Spin Rotation: Principles and Applications in Solid State Physics* (Hilger, Bristol, Boston, 1985).
- [27] J. H. Brewer, in *Encyclopedia of Applied Physics*, Vol. 11, edited by G. L. Trigg, E. S. Vera, and W. Greulich (VCH Publishers, New York, 1994) pp. 23–53.
- [28] A. Yaouanc and P. Dalmas de Réotier, *Muon Spin Rotation, Relaxation, and Resonance: Applications to Condensed Matter*, Vol. 147 (Oxford University Press, 2011).
- [29] N. H. Sung, H. Gretarsson, D. Proepper, J. Porras, M. Le Tacon, A. V. Boris, B. Keimer, and B. J. Kim, *Phil. Mag.* **96**, 413 (2016).
- [30] T. F. Qi, O. B. Korneta, L. Li, K. Butrouna, V. S. Cao, X. Wan, P. Schlottmann, R. K. Kaul, and G. Cao, *Phys. Rev. B* **86**, 125105 (2012).
- [31] R. S. Hayano, Y. J. Uemura, J. Imazato, N. Nishida, T. Yamazaki, and R. Kubo, *Phys. Rev. B* **20**, 850 (1979).
- [32] Y. J. Uemura, T. Yamazaki, D. R. Harshman, M. Senba, and E. J. Ansaldo, *Phys. Rev. B* **31**, 546 (1985).

- [33] R. Kubo and T. Toyabe, in *Magnetic Resonance and Relaxation*, edited by R. Blinc (North-Holland, Amsterdam, 1967) pp. 810–823.
- [34] C. P. Slichter, *Principles of magnetic resonance*, Vol. 1 (Springer Science & Business Media, 2013).
- [35] Y. Aoki, A. Tsuchiya, T. Kanayama, S. R. Saha, H. Sugawara, H. Sato, W. Higemoto, A. Koda, K. Ohishi, K. Nishiyama, and R. Kadono, *Phys. Rev. Lett.* **91**, 067003 (2003).
- [36] The holder in a μ SR spectrometer is usually made of pure silver, because of its good thermal conductivity and because the absence of strong nuclear magnetism simplifies its μ SR signal.
- [37] J. P. Clancy, A. Lupascu, H. Gretarsson, Z. Islam, Y. F. Hu, D. Casa, C. S. Nelson, S. C. LaMarra, G. Cao, and Y.-J. Kim, *Phys. Rev. B* **89**, 054409 (2014).
- [38] J. F. Bueno, D. J. Arseneau, R. Bayes, J. H. Brewer, W. Faszer, M. D. Hasinoff, G. M. Marshall, E. L. Mathie, R. E. Mischke, G. D. Morris, K. Olchanski, V. Selivanov, and R. Tacik, *Phys. Rev. B* **83**, 205121 (2011).
- [39] C. M. Varma, *J. Phys. Condens. Matter* **26**, 505701 (2014).
- [40] N. Bloembergen, E. M. Purcell, and R. V. Pound, *Phys. Rev.* **73**, 679 (1948).
- [41] O. O. Bernal, D. E. MacLaughlin, G. D. Morris, P.-C. Ho, L. Shu, C. Tan, J. Zhang, Z. Ding, K. Huang, and V. V. Poltavets, *Phys. Rev. B* **100**, 125142 (2019).
- [42] V. G. Grebinnik, I. I. Gurevich, V. A. Zhukov, A. P. Manych, E. A. Meleshko, I. A. Muratova, B. A. Nikol'skii, V. I. Selivanov, and V. A. Suetin, *Zh. Eksp. Teor. Fiz.* **68**, 1548 (1975), [*Sov. Phys.–JETP* **41**, 777 (1976)].